Spherical gear coupling design space analysis for high misalignment applications

Aurea Iñurritegui[a,*], Aitor Arana[a], Jon Larrañaga[a], Ibai Ulacia[a]

[a]*Mondragon Unibertsitatea, Department of Mechanical and Industrial Production, Arrasate-Mondragon, Pais Vasco, SPAIN*

Abstract

Spherical gear couplings are machine elements that enable power transmission between highly misaligned shafts. The highly crowned tooth surfaces and the presence of undercut sections, have been a matter of disagreement between existing geometry generation methods available in the scientific literature. The main reason for this, are the geometry variations which arise in the generated parts, and consequently, the effect of such variations on the contact point location and clearance distribution. In this paper the influence of the main design parameters of spherical gear couplings (namely, the crowning ratio, the pitch diameter, the pressure angle, etc.), on the geometrical properties of the gear tooth surfaces are investigated. An algorithm to calculate the maximum misalignment angle is proposed, which is one of the most crucial design parameters. It shows that the values obtained with models existing in the literature are not applicable to highly crowned spherical gear couplings. Finally, design criteria are described to help the designer choose proper spherical gear coupling tooth geometry parameters to fit in a certain space and achieve a given maximum misalignment angle without further geometrical issues (undercut or pointed teeth).

Keywords: spherical gear coupling, high misalignment, main design parameter limits

*Corresponding author

Email address: ainurritegui@mondragon.edu (Aurea Iñurritegui)

Nomenclature

a_p	parabola coefficient for profile crowning
b	hub face width
$C_{h\beta}$	amount of longitudinal crowning in the hub
$D_{\text{ext, h}}$	external diameter of the hob
h_{ha}	hub addendum coefficient
h_{hf}	hub dedendum coefficient
j	clearance
k	clearance factor
m_n	normal module
N_w	number of threads of the hob
r_c	hub crowning radius
r_p	hub pitch radius
$r_{p,w}$	hob pitch radius
r_t	hub tooth transverse crowning radius
r_β	tool path radius
s_c	sleeve space width
s_w	hob displacement during hub generation
t_c	hub tooth width
u	profile surface parameter
v	lead surface parameter
x_{sleeve}	profile shift coefficient of the sleeve
z	number of teeth of the hub
α	pressure angle
γ	misalignment angle
Δ_{hw}	vertical displacement of the hob during generation
$\Delta\gamma$	misalignment angle variation
ε	crowning ratio
λ_{w}	hob lead angle
μ	angle along hob tool path
ρ_{hf}	hub root radius coefficient
Σ_c	rack-cutter tooth surface
Σ_h	generated hub tooth surface
Σ_w	generating hob-thread tooth surface
ϕ_w	hob rotation during hub generation
ψ_h	generation parameter of the hub
ψ_w	generation parameter of the hob

1. Introduction

Gear couplings are widely used to transmit power between shafts due to their high power density compared to other non-splined connections and their capacity to accommodate axial, radial or angular misalignments [1]. Usually, they are employed in applications where, due to the working conditions, slight misalignment occurs between the axes [2] or manufacturing uncertainties exist [3]. In contrast, spherical gear couplings are specially designed to transmit power between highly misaligned shafts, $\gamma \in \mathbb{R} : 3^\circ \leq \gamma \leq 10^\circ$. They are composed of a highly crowned toothed hub (external part) and a commonly straight [4, 5] sleeve (internal part), both of which have the same number of teeth, as it can be seen in Fig. 1.

Spherical gear couplings are used in heavy duty, high torque applications [6], such as in sheet metal rolling mills [7], where due to the small roller size, working conditions of up to 7° misalignment angle can be found [8]. In

these applications, the large longitudinal crowning of spherical gear couplings, enables a favorable contact pattern [6]. In addition, it balances the clearance between the tooth surfaces to prevent interference between the teeth [3].

To attain the tooth geometry which enables the described working kinematics, hubs are manufactured by hobbing. Generation by a disc is also mentioned in the literature [4, 5], however this process is never used to generate sufficient crowning to withstand such high misalignment angles (above 3°). The tooth geometry of the gear coupling is obtained from the combination of the cutter tooth geometry and the kinematics of the machining process. Most of the mathematical approaches existing in the literature simplify the hobbing process, modeling only its central cutting edge [5, 9, 10, 11]. However, these methods do not consider the threaded surface of the hob (a set of cutting edges distributed along its thread) during the generation. Thus, even if they may be accurate enough for tooth geometries with small amounts of crowning, they present strong deviations when generating highly crowned spherical hub tooth surfaces, as shown by the authors in [12].

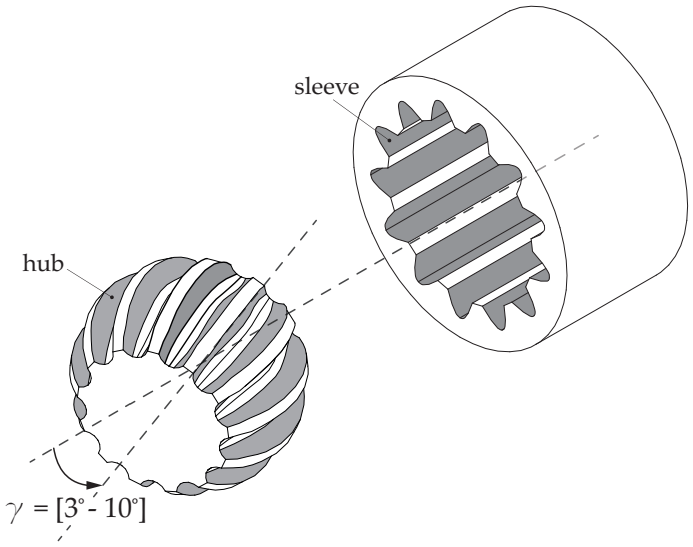

Figure 1: Spherical gear coupling: highly crowned hub and straight sleeve.

In accordance with design criteria and assuming that misalignment is an unavoidable condition, many studies have focused on different aspects of the operating conditions of gear couplings. Alfares et al. [3] showed that the main factors influencing the clearance distribution were the misalignment angle, the tooth surface longitudinal crowning, and the tooth angular position. Hong et al. [13] analyzed the effect of variable clearance distribution due to indexing errors, revealing that tighter manufacturing tolerances exhibit more favorable load sharing characteristics. From this and other similar studies, it has been shown that the contact position moves farther away from the middle section to the edge as misalignment increases, generating undesired load concentrations. For this reason, the main objective of the crowned surface is to prevent edge contact and to center the contact between the hub and the sleeve [3, 14, 15]. This is achieved by tooth surface geometry upgrades. For instance, early studies [14], propose the Vari-Crown geometry, which increases the contact area significantly, by means of a variable crowning radius along the face width, with the maximum radii being at the load angle. More recently, Guan et al. [15] introduced a novel crown gear coupling, which contains profile crowning in the teeth, together with longitudinal crowning, to center the point of contact. In fact, due to the issues caused by load concentrations in gear couplings, design standards, such as AGMA 945-1-B20 [16, 17], limit the tooth surface geometry up to the point where undercutting sections exist [18]. Therefore, geometries with undercutting singularities are discarded in the design phase of spherical gear couplings.

Previous works have provided a great insight into the performance of gear couplings, however they have been mainly focused on small misalignment angles ($\gamma \ll 3°$). Very few papers can be found concerning high misalignment angle applications. Herbstritt and Paluh [19] correlated numerical models with experimental tests showing a considerable effect of the misalignment angle (3°) on tooth bending stresses. Moreover, Ulacia et al. [8] compared tooth root bending fatigue life of spherical couplings at 7° with the stress value obtained with a measured tooth geometry finite

element model. All these works have shown the impact of the tooth geometry on tooth stresses and the life of gear couplings, however to the best of the authors knowledge, no design guidelines exist for high misalignment applications. Moreover, the existing standards, DIN 5466 [20], ISO 4156 [17], AGMA 6123-B06 [21] and AGMA 945-1-B20 [16] are mainly focused on small misalignments, and spherical gear couplings for high misalignment applications are referred to as special cases.

Therefore, this paper presents a comprehensive approach to determine the influence of the main design parameters of spherical gear couplings on the achievable misalignment angle, to help manufacturers and designers in a first approach of the design phase. To this end, the main goals of this research are:

(1) Propose an algorithm to determine the maximum misalignment angle in spherical gear couplings based on the generated geometry, and compare them with the results obtained with existing analytical methods from the literature.

(2) Apply the mathematical generation model of spherical gear couplings proposed in [12] to investigate the influence of the main design parameters on the hub tooth surface geometry and achievable maximum misalignment angle.

(3) Determine the preliminary design space which fulfills the required maximum misalignment angle and available space of the application. This will provide the designer with spherical gear coupling geometries, preventing as much as possible tooth surface geometry issues, such as undercutting or tip pointing.

2. Mathematical model to generate spherical hub tooth surfaces

The mathematical hobbing of spherical gear couplings manufacturing process is considered here. Throughout this process, the hob follows a circular feeding motion, where the center distance between the gear and the hob varies continuously. The maximum value of the center distance is equal to the sum of the gear couplings r_p and hobs r_h pitch radii (Fig. 2). The spherical hub tooth surfaces are generated considering the hob thread surface as a set of cutting edges acting at the same time during the generation process, as explained in [12]. Figure 2 shows a schematic representation of the complete generation process, where the hob thread surface is determined prior to the generation of the hub with the hob.

The generating rack cutter profile is defined in coordinate system S_a as:

$$\mathbf{r}_{\mathrm{a}}(u) = [u \quad 0 \quad 0 \quad 1]^{\mathrm{T}} \tag{1}$$

where u is the surface parameter in the profile direction.

To prevent edge contact at the tips of the hub and sleeve teeth in presence of a high misalignment angle, profile crowning is required and $\mathbf{r}_{\mathrm{a}}(u)$ vector is obtained as:

$$\mathbf{r}_{\mathrm{a}}(u) = [u \quad a_p u^2 \quad 0 \quad 1]^{\mathrm{T}} \tag{2}$$

where a_p is a parabola coefficient, and in this work takes a value of $a_p = 0.001\ \mathrm{mm}^{-1}$.

The rack cutter generating tooth surface Σ_c is represented in coordinate system S_c as:

$$\mathbf{r}_{\mathrm{c}}(u, v) = \mathbf{M}_{\mathrm{cb}}(v)\, \mathbf{M}_{\mathrm{ba}}\, \mathbf{r}_{\mathrm{a}}(u) \tag{3}$$

where matrix $\mathbf{M}_{\mathrm{cb}}$ and $\mathbf{M}_{\mathrm{ba}}$ are coordinate transformation matrix and v is the other surface parameter in the feed direction.

The rack cutter tooth proportions for gear couplings in this research are defined in accordance to the pressure angle value as shown in Table 1.

Coordinate transformation (4) from system S_c to system S_w and consideration of the meshing equation (5) allows the determination of the hob thread surface Σ_w from the rack-cutter tooth surface Σ_c:

$$\mathbf{r}_{\mathrm{w}}(u, v, \psi_w) = \mathbf{M}_{\mathrm{wm}}(\psi_w)\, \mathbf{M}_{\mathrm{mc}}\, \mathbf{r}_{\mathrm{c}}(u, v) \tag{4}$$

$$f_1(u, v, \psi_w) = \left(\frac{\partial \mathbf{r}_{\mathrm{w}}}{\partial u} \times \frac{\partial \mathbf{r}_{\mathrm{w}}}{\partial v} \right) \cdot \frac{\partial \mathbf{r}_{\mathrm{w}}}{\partial \psi_w} = 0 \tag{5}$$

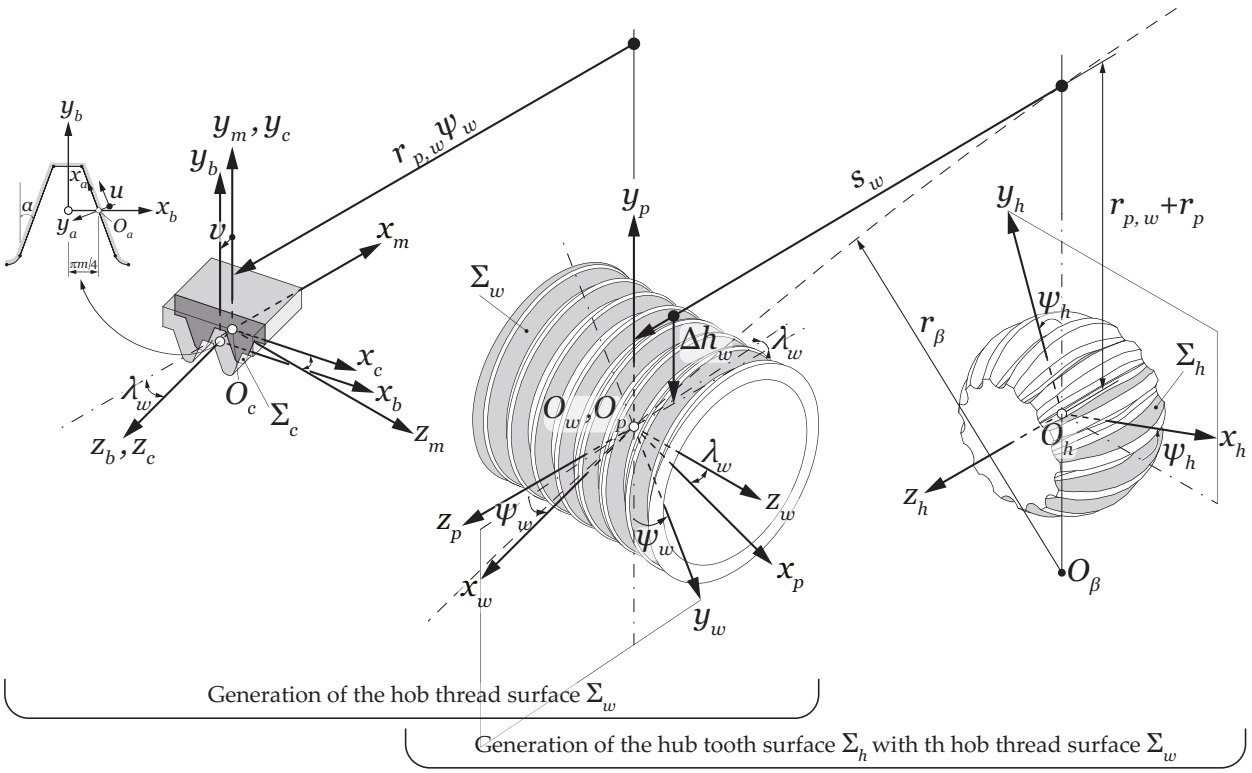

Figure 2: Derivation of the hub tooth surface Σ_h, with the prior determination of the hob thread surface Σ_w.

Table 1: Hub tooth proportion coefficients in accordance with ISO 4156 [17] and Beckmann [22].

Parameter	**Values**			
Pressure angle, α	20°	30°	37.5°	45°
Addendum coeff., h_{ha}	0.50	0.50	0.45	0.40
Deddendum coeff., h_{hf}	0.90	0.90	0.70	0.60
Root radius coeff., ρ_{hf}	0.40	0.40	0.30	0.25

Here, ψ_w is the generation parameter for the hob thread surface and matrices $\mathbf{M}_{\mathrm{wm}}$ and $\mathbf{M}_{\mathrm{mc}}$ are the coordinate transformation matrix.

The external diameter $D_{\mathrm{ext,h}}$ of the hob thread Σ_w is based on the geometry of the hub that will be generated. Standard AGMA 1102-A03 [23] defines the external diameter in terms of the generated hub geometry modulus as shown in Table 2. The rest of the tool parameters, such as, the lead angle are defined depending on it.

Table 2: Hob external diameter $D_{\mathrm{ext,h}}$ definition in terms of the module in accordance with AGMA 1102-A03 [23].

m_n	0.5	1.0	1.5	2.0	3.0	4.0	5.0	6.0	8.0	10.0
$D_{\mathrm{ext,h}}$	32	50	55	65	75	85	95	105	120	130

Coordinate transformation (6) from system S_w to system S_h and consideration of a double-enveloping process [24] with two independent parameters of generation ϕ_w and s_w (7, 8) enables to determine the hub tooth surface Σ_h by the rotation of the hob thread surface along a curved tool path:

$$\mathbf{r}_{\mathrm{h,a}}(u, v, \psi_w, s_w, \phi_w) = \mathbf{M}_{\mathrm{hp}}(s_w, \phi_w)\, \mathbf{M}_{\mathrm{pw}}\, \mathbf{r}_{\mathrm{w}}(u, v, \psi_w) \tag{6}$$

$$f_2(u, v, s_w, \phi_w) = \left(\frac{\partial \mathbf{r}_{\mathrm{h,a}}}{\partial u} \times \frac{\partial \mathbf{r}_{\mathrm{h,a}}}{\partial v}\right) \cdot \frac{\partial \mathbf{r}_{\mathrm{h,a}}}{\partial \phi_w} = 0 \tag{7}$$

$$f_3(u, v, s_w, \phi_w) = \left(\frac{\partial \mathbf{r}_{\mathrm{h,a}}}{\partial u} \times \frac{\partial \mathbf{r}_{\mathrm{h,a}}}{\partial v}\right) \cdot \frac{\partial \mathbf{r}_{\mathrm{h,a}}}{\partial s_w} = 0 \tag{8}$$

Here, $\mathbf{M}_{\mathrm{hp}}$ and $\mathbf{M}_{\mathrm{pw}}$ are given by:

$$\mathbf{M}_{\mathrm{hp}} \cdot \mathbf{M}_{\mathrm{pw}} = \begin{bmatrix} \cos\psi_h & \sin\psi_h & 0 & 0 \\ -\sin\psi_h & \cos\psi_h & 0 & r_{\mathrm{p,h}} + r_{\mathrm{p,w}} - \Delta h_w \\ 0 & 0 & 1 & s_w \\ 0 & 0 & 0 & 1 \end{bmatrix} \cdot \begin{bmatrix} \cos\psi_w \sin\lambda_w & -\sin\lambda_w \sin\psi_w & \cos\lambda_w & 0 \\ -\sin\psi_w & -\cos\psi_w & 0 & 0 \\ \cos\lambda_w \cos\psi_w & -\cos\lambda_w \sin\psi_w & -\sin\lambda_w & 0 \\ 0 & 0 & 0 & 1 \end{bmatrix} \tag{9}$$

where $r_{\mathrm{p,h}}$ is the hub pitch radius, $\psi_h = \phi_w \cdot (N_w/z)$ is the rotation of the hub during generation, and N_w and z represent the number of threads in the hob and the number of teeth in the hub respectively. $\Delta h_w = r_\beta - \sqrt{r_\beta^2 - s_w^2}$ determines the plunging of the hob when a circular tool path of radius r_β is applied. Indeed, Δh_w will vary depending on the tool path function used.

The simultaneous consideration of equation (6) and equations of meshing (5, 7, 8) enables the hub tooth surface to be generated from the rack cutter surface and hob tooth surface definition.

The generation of the fillet hub tooth surface $\Sigma_{\mathrm{h,f}}$ can be obtained following a similar approach to the one described along this section, but it is omitted here for the purpose of simplicity. Moreover, the sleeve generation model is based on involute tooth surfaces and point contact is assumed between hub and sleeve tooth surfaces, due to the double crowned tooth surfaces of the hub. The detailed information of the computerized generation of highly crowned spherical gear couplings and all the coordinate transformation matrix can be found in [12].

3. Determination of the maximum misalignment angle

3.1. Crowning radius r_c and misalignment angle γ relationship

It has been shown that most of the research in the literature is focused on small misalignment angles and that works referring to misalignment angles above 3° are rare. Moreover, references [22, 25, 26] do mention the existence of gear couplings for larger misalignment angles, but recommend design guidelines only for $\gamma \leq 1.5°$. At the same time, they note that designs for misalignment angles above 1.5° are special cases, and deviate from the generalities discussed for small misalignment designs.

The amount of longitudinal crowning ($C_{h\beta}$) (Fig. 3(b)) is a key parameter to determine the maximum misalignment angle in several works [2, 3, 27]. However, it is not straightforward to obtain in highly crowned spherical hubs, due to the small tool path radius used in their manufacturing [12]. For this reason, a more suitable parameter related to the manufacturing process should be used to determine the maximum misalignment angle. A more appropriate parameter for this purpose is the crowning radius r_c. This is related to the generated hub geometry and the manufacturing tool path radius, as can be observed in Fig. 3(a). This figure also illustrates the relationship between the pitch radius r_p, the hob pitch radius $r_{p,w}$, crowning radius r_c, and tool path radius r_β, all defined in the pitch-plane of the hub. For a given hub and hob pitch radius, the tool path variation will require a direct change of the crowning radius r_c, and in consequence, in the amount of longitudinal crowning $C_{h\beta}$ generated. At the same time, $C_{h\beta}$ will involve a modification of the maximum attainable misalignment angle $\gamma_{\max}$.

Nevertheless, there are few references that analytically calculate the maximum misalignment angle of spherical gear couplings. This may be due to the predominant use of gear couplings in applications working at small misalignment angles, where the major objective of the crowned surface is the prevention of edge contact and the centering of the contact between the hub and the sleeve.

Among the equations found to define the maximum misalignment angle, those including mathematical simplifications related to small misalignment angles were disregarded [27]. Relevant equations for this analysis include equations that consider tooth design parameters, such as the crowning radius and the module and the clearance value, among others. Thus, the most relevant references that could be applied to high misalignment cases are equations (10, 11) from Beckmann [22] and Guo et al. [2], respectively. It should also be noted that these equations were only used in small misalignments, below 1.5°. All in all, it can be observed that eqn. (10) is in terms of the clearance value

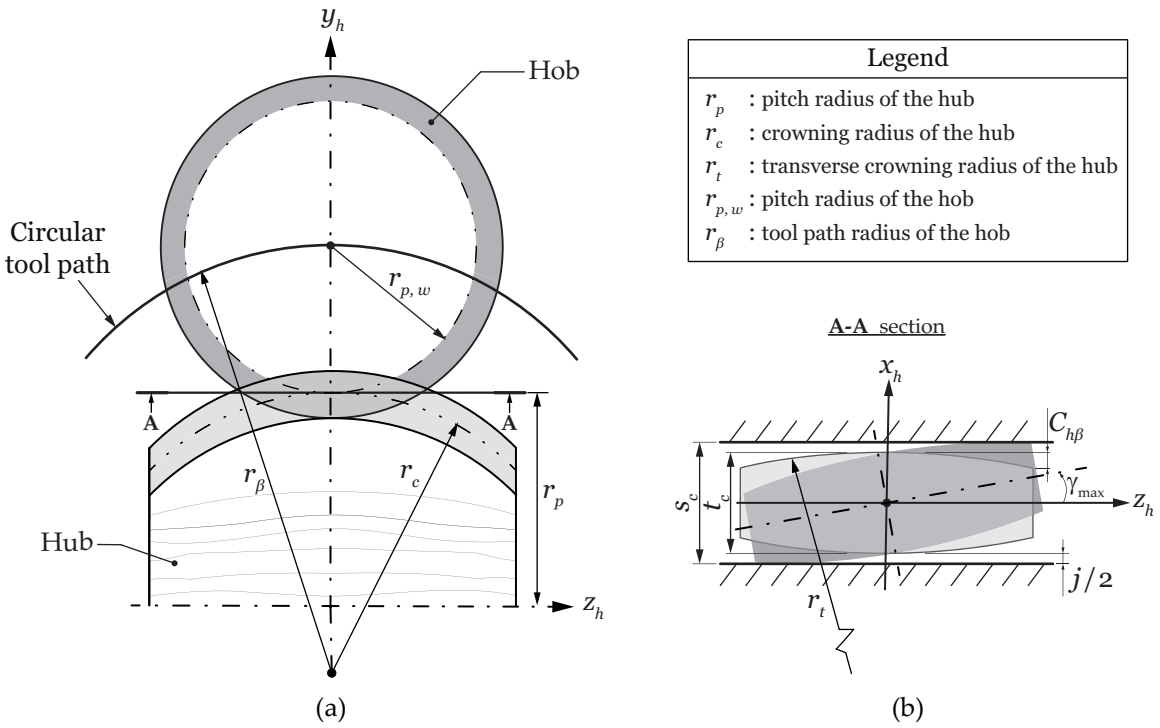

Figure 3: (a) Definition of characteristic radii in highly crowned hub generation, and (b) pitch-plane of the hub teeth with relevant parameters for the definition of the maximum misalignment angle.

between the hub and sleeve, while eqn. (11) does not consider it, and in contrast, includes among its variables the gear coupling face width b.

$$\gamma = \arccos\left(1 - \frac{2km_n \tan(\alpha)}{4r_c - \pi m_n tan(\alpha)}\right) \tag{10}$$

$$\gamma = \arcsin\left(b\frac{\tan(\alpha)}{2r_c}\right) \tag{11}$$

Moreover, a dimensionless parameter relating the generated geometry (r_p) with the hobbing process (r_c) (see eqn. (12)) is proposed in the literature [22, 26]. This coefficient, named the crowning ratio ε, relates the gear coupling size (the pitch radius r_p) and the crowning radius r_c, and thus is employed in this work to generate equivalent/comparable geometries in terms of the size and amount of crowning.

$$\varepsilon = r_c/r_p \tag{12}$$

To calculate the maximum misalignment angle, a clearance value between the hub and sleeve has to be defined. This is defined following [22], and is proportional to the module as shown in eqn. (13).

$$j = k \cdot m_n \tag{13}$$

In this research, no profile shift coefficient is employed in the hub, to ensure that this parameter has no influence on the results. In contrast, to ensure the clearance value between the hub and the sleeve, the profile shift coefficient calculated with eqn. (14) is entirety applied to the sleeve.

$$x_{\text{sleeve}} = \frac{j/2}{m_n \sin(\alpha)} = \frac{k}{2\sin(\alpha)} \tag{14}$$

3.2. Algorithm to determine the maximum misalignment angle $\gamma_{\max}$

To define the maximum applicable misalignment angle of the generated hub, Fig. 4(a) depicts a fixed coordinate system S_f where the hub and sleeve tooth surface models are assembled. The system S_h is rigidly connected to the hub and mounted in the system S_f, enabling a misalignment angle around the axis y_f, which coincides with the axis y_h. Both models are held at rest without load and no rotation is imposed on either of them. The standard AGMA 6123-B06 [21] and Guo et al. [2] use the jam angle to determine the geometrical maximum misalignment angle. This is defined as, the angle at which both sides of the hub tooth surfaces contact the sleeve and, therefore, the component becomes blocked. This can be observed in Fig. 3(b), where the maximum misalignment angle is defined in such an angle where contact exists in both sides of the hub tooth surfaces. Thus, a designer must ensure that the jam angle is greater or equal to the misalignment expected during operation. To determine the maximum misalignment angle, a clockwise and counterclockwise angle is applied to consider tooth geometry variations [12] which can occur due to the lead angle (twist effect) [28].

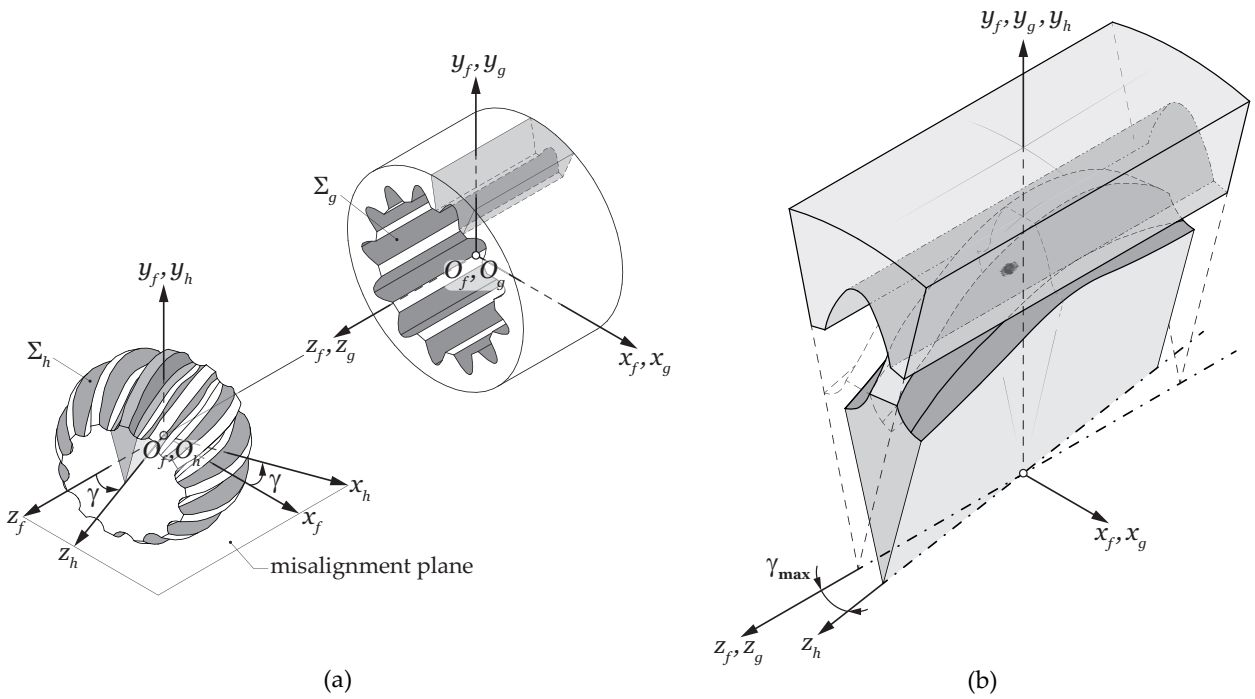

Figure 4: Maximum misalignment angle determination: (a) Coordinate systems for the positioning of the gear coupling with shaft misalignment γ, and (b) simplification of the teeth and contact in pure tilting position at 0°.

The following algorithm, divided into 5 steps, is applied to determine the contact point between the pair of teeth located in the tilting position (Fig. 4(b)) and deduce the maximum misalignment angle of the spherical gear coupling. The tooth in the tilting position is considered to be critical, as it is the first which comes into contact [3, 12, 22].

Step 1 The tooth of the hub whose symmetry axis is perpendicular to the misalignment plane, in the tilting position, is selected. A counter-clockwise rotation of the hub is considered to find the misalignment angle γ. Assuming, for the purpose of simplicity, that $(u_\mathrm{h}, v_\mathrm{h})$ are the surface parameters of surface Σ_h, the following coordinate transformation (15) allows the surface Σ_h to be represented in the system S_f:

$$\mathbf{r}_\mathrm{f}^{(\mathrm{hub})}(u_\mathrm{h}, v_\mathrm{h}, \gamma) = \mathbf{M}_\mathrm{fh}\mathbf{r}_\mathrm{h}(u_\mathrm{h}, v_\mathrm{h}) \tag{15}$$

Here, $\mathbf{M}_{\mathrm{fh}}$ is given by:

$$\mathbf{M}_{\mathrm{fh}} = \begin{bmatrix} \cos\gamma & 0 & \pm\sin\gamma & 0 \\ 0 & 1 & 0 & 0 \\ \mp\sin\gamma & 0 & \cos\gamma & 0 \\ 0 & 0 & 0 & 1 \end{bmatrix} \tag{16}$$

where γ is the angle of misalignment and the upper and lower signs are applied to a clockwise and a counterclockwise rotation, respectively. The variables $(u_{\mathrm{h}}, v_{\mathrm{h}}, \gamma)$ are the unknowns for the sought-for contact point.

Step 2 The unit normal to surface Σ_h at the sought-for contact point can be obtained in the system S_f as:

$$\mathbf{n}_{\mathrm{f}}^{(\mathrm{hub})}(u_{\mathrm{h}}, v_{\mathrm{h}}, \gamma) = \mathbf{L}_{\mathrm{fh}} \frac{\dfrac{\partial \mathbf{r}_{\mathrm{h}}}{\partial u_{\mathrm{h}}} \times \dfrac{\partial \mathbf{r}_{\mathrm{h}}}{\partial v_{\mathrm{h}}}}{\left| \dfrac{\partial \mathbf{r}_{\mathrm{h}}}{\partial u_{\mathrm{h}}} \times \dfrac{\partial \mathbf{r}_{\mathrm{h}}}{\partial v_{\mathrm{h}}} \right|} \tag{17}$$

where the matrix $\mathbf{L}_{\mathrm{fh}}$ is of 3×3 order and can be determined from the matrix $\mathbf{M}_{\mathrm{fh}}$ by removing the last row and the last column.

Step 3 The tooth surface of the sleeve Σ_{g} comes into contact with the surface Σ_{h}, defined by surface parameters $(u_{\mathrm{g}}, v_{\mathrm{g}})$, for the purpose of simplicity. As the sleeve is held at rest, surface Σ_{g} is represented in the system S_f as:

$$\mathbf{r}_{\mathrm{f}}^{(\mathrm{sleeve})}(u_{\mathrm{g}}, v_{\mathrm{g}}) = \mathbf{r}_{\mathrm{g}}(u_{\mathrm{g}}, v_{\mathrm{g}}) \tag{18}$$

where $(u_{\mathrm{g}}, v_{\mathrm{g}})$ are the unknowns of the sought-for contact point.

In the same way, the unit normal to surface Σ_{g} at the sought-for contact point is obtained in the system S_f as:

$$\mathbf{n}_{\mathrm{f}}^{(\mathrm{sleeve})}(u_{\mathrm{g}}, v_{\mathrm{g}}) = \frac{\dfrac{\partial \mathbf{r}_{\mathrm{g}}}{\partial u_{\mathrm{g}}} \times \dfrac{\partial \mathbf{r}_{\mathrm{g}}}{\partial v_{\mathrm{g}}}}{\left| \dfrac{\partial \mathbf{r}_{\mathrm{g}}}{\partial u_{\mathrm{g}}} \times \dfrac{\partial \mathbf{r}_{\mathrm{g}}}{\partial v_{\mathrm{g}}} \right|} \tag{19}$$

Step 4 A system of five independent scalar equations with the unknowns $\{ u_{\mathrm{h}}, v_{\mathrm{h}}, \gamma, u_{\mathrm{g}}, v_{\mathrm{g}} \}$ is defined as:

$$\mathbf{r}_{\mathrm{f}}^{(\mathrm{hub})}(u_{\mathrm{h}}, v_{\mathrm{h}}, \gamma) = \mathbf{r}_{\mathrm{f}}^{(\mathrm{sleeve})}(u_{\mathrm{g}}, v_{\mathrm{g}}) \tag{20}$$

$$\mathbf{n}_{\mathrm{f}}^{(\mathrm{hub})}(u_{\mathrm{h}}, v_{\mathrm{h}}, \gamma) = \mathbf{n}_{\mathrm{f}}^{(\mathrm{sleeve})}(u_{\mathrm{g}}, v_{\mathrm{g}}) \tag{21}$$

In fact, eqn. (21) represents only two independent scalar equations since $|\mathbf{n}_{\mathrm{f}}^{(\mathrm{hub})}| = |\mathbf{n}_{\mathrm{f}}^{(\mathrm{sleeve})}| = 1$.

Step 5 Steps 1 to 4 are repeated for a clockwise rotation. That way, the geometry deviations related the twist-effect are also considered [12, 28]. The smallest value of both is established to be the maximum misalignment angle of the gear coupling.

4. Conditions of existence for spherical gear couplings working in high misalignment applications

In the following subsections, three tooth surface geometry existence conditions are presented to evaluate the quality of the generated hub tooth surfaces. The first two, pointed teeth and undercut, are commonly used for gears and are taken into account in gear coupling standards [16, 17] while the third, is a new parameter proposed for highly crowned spherical gear couplings.

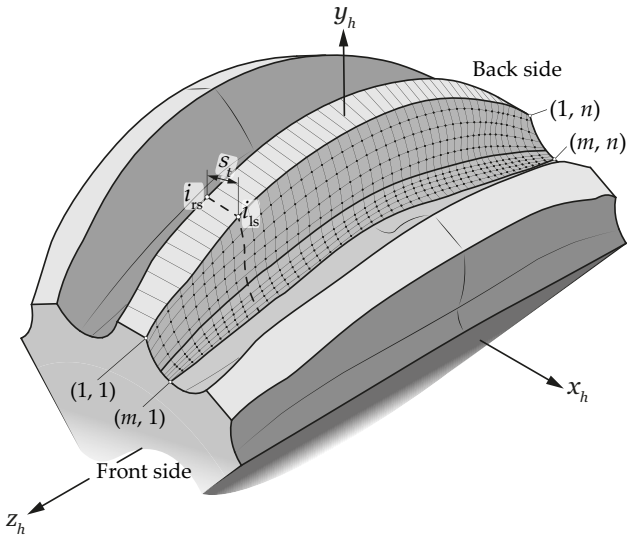

Figure 5: Determination of the tip width s_t.

4.1. Pointed teeth

Figure 5 shows the definition of the tip width (s_t) of the spherical hub tooth surfaces, where the tooth flanks are discretized into $m \times n$ points. m represents the number of points across the tooth profile direction and n the number of points along the face width direction of the hub flank. As shown in Fig. 5, a point in the addendum edge and the front side of the tooth is defined as $(1, 1)$ and a point at the root and back side is defined as (m, n).

For spherical crowned hubs, apart from the geometry parameters (d_p, α, etc.) of the generated hub, the crowning radius plays a significant role in the tip width (Fig. 6(a)). Similar to the general rule specified for cylindrical gears, ISO 4156 [17] states the following equation (22) for the tip thickness limit.

$$s_{t,n} \geq 0.25 \cdot m_n \tag{22}$$

Tip width $s_{t,n}$ refers to the distance between right side i_{rs} and left side i_{ls} top points of each n section, which can be represented as:

$$s_{t,n} = \sqrt{(x_{i,\mathrm{rs}} - x_{i,\mathrm{ls}})^2 + (y_{i,\mathrm{rs}} - y_{i,\mathrm{ls}})^2 + (z_{i,\mathrm{rs}} - z_{i,\mathrm{ls}})^2} \tag{23}$$

where $(x_{i,\mathrm{rs}}, y_{i,\mathrm{rs}}, z_{i,\mathrm{rs}})$ and $(x_{i,\mathrm{ls}}, y_{i,\mathrm{ls}}, z_{i,\mathrm{ls}})$ denote the coordinates of points i_{rs} and i_{ls} in the fixed coordinate system S_f. The range for index i goes from 1 to n. The right and left side profiles are limited to the positive and negative side of the S_h coordinate system, respectively, to prevent crossover.

4.2. Undercut profiles

Using the algorithm described in [12] the undercutting and only-fillet regions can be detected and the length of the face width at which they appear can be determined. Indeed, when tangency no longer exists between the active profile $\Sigma_{h,a}$ and the fillet $\Sigma_{h,f}$, a singularity occurs and the profiles are undercut (Fig. 6(a)).

4.3. Useful flank

The relative slenderness of the gear coupling is called the aspect ratio. It is a dimensionless coefficient which relates the face width b and the pitch diameter d_p of the gear coupling; that is to say, the stiffness of the teeth of the hub. For this reason, in the gear coupling standard DIN 5466 [20], it is used for the calculation of the bending moment, torsional moment, and surface maximum pressure, among other strength parameters.

However, for highly crowned spherical hubs, the length of the hub b is not equivalent to the length of the active profile b_{flank} as shown in Fig. 6(b). Indeed, sections with only-fillet profiles might occur as was presented in [12].

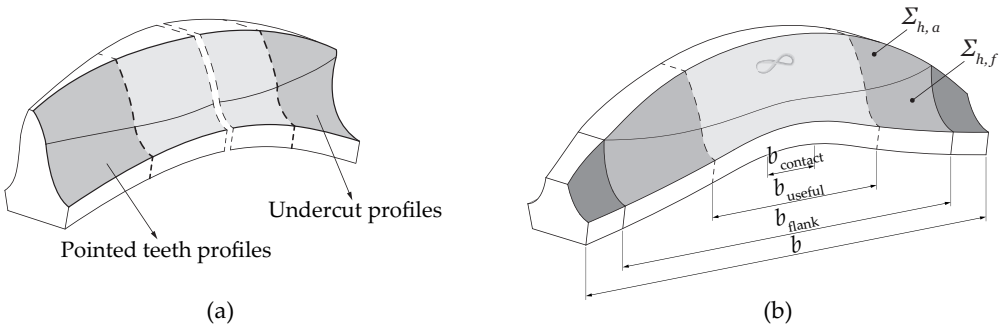

Figure 6: Hub geometry characteristics: (a) undercut and pointed teeth profiles, and (b) gear coupling face width b, active profile length b_{flank}, length of no undercutting or pointed teeth flank b_{useful}, and contact length b_{contact} definitions.

Moreover, AGMA 945-1-B20 [16] defines the concept of the axial engagement length, referring to the b_{contact} in Fig. 6(b), and recommends this distance to be as great as possible to reduce contact, shear and bending stresses. Thus, in this study, with the purpose of comparing different geometries and determining whether they are geometrically more appropriate to withstand a given misalignment, two dimensionless parameters are defined:

- The flank ratio: b_{flank}/d_p
- The useful flank ratio: b_{useful}/d_p

The lengths are indicated in Fig. 6(b), where b_{flank} corresponds to the length of the face width containing an active profile, and b_{useful} to the length of the active profile without undercut or pointed teeth.

Between two equivalent geometries, that with the largest value of useful flank ratio should be chosen, as it will provide better contact surface and stiffness to the gear coupling. In the same way, a hub with the same aspect ratio, flank ratio and useful flank ratio that fulfills the design criteria will be the ideal geometry for the target application.

5. Definition of the cases of study

In this study two types of analysis were done: (a) a comparison of the method to calculate the misalignment angle with scientific literature models, and (b) influence of geometry variables.

5.1. Comparison with the scientific literature models

To analyze how maximum misalignment angle is determined in the scientific literature and compare it with the model proposed here, four gear coupling geometries from the literature (**L**) and four representative case studies (**CS**) were defined as shown in Table 3. This table contains all the design characteristics, along with the maximum misalignment angle for which the different literature models (**L**) were analyzed in the literature, and the maximum misalignment angle of the proposed case studies (**CS**), calculated with the model in Section 2.

On the one hand, the literature models (**L**) chosen are considered as references that have recently worked in misaligned crowned gear couplings. The first is a straight gear hub **L1** defined by Xiao et al. 2022 [29], while the rest are geometries with larger crowning ratios: **L2** by Hong et al. 2015 [30], **L3** by Guo et al. 2016 [2] and **L4** from Guan et al. 2021 [31]. It should be pointed out that **L1** is a straight gear coupling which consequently will exhibit edge contact when misalignment is present, unlike the rest of the cases analyzed here.

On the other hand, the case studies (**CS**) were chosen to clearly show the differences between equations (10,11) and the proposed model, considering the influence of the crowning ratio and the size. **CS1** and **CS2** represent relatively high crowning ratio geometries in the context of the present study, but low within the scientific literature. In contrast, **CS3** and **CS4** are highly crowned hubs (small crowning ratio). Moreover, **CS2** and **CS4** refer to small pitch diameter gear couplings, while **CS1** and **CS3** represent big diameters. Thus, these four cases are selected to showcase the influence of the crowning ratio on the calculated misalignment angle.

Table 3: Gear coupling geometry parameters for misalignment angle comparison.

Parameter	**L1**	**L2**	**L3**	**L4**	**CS1**	**CS2**	**CS3**	**CS4**
d_p [mm]	75	79	1016	120	99	51	99	51
m_n [mm]	2.50	3.175	10.16	3	3	3	3	3
z [-]	30	25	100	40	33	17	33	17
α [°]	20	30	20	20	30	30	30	30
b/d_p	0.367	0.625	0.125	0.150	0.30	0.30	0.30	0.30
j [mm]	0.50	0.62	0.64	0.71	0.71	0.71	0.71	0.71
ε [-]	∞	62.99	3.94	1.67	1.00	1.00	0.40	0.40
$\gamma_{\max}$ [°]	0.20	0.06	0.80	0.80	4.50	4.75	2.94	7.90
Tool path shape	Circular							
$D_{\text{ext,h}}$ [mm]	$f(m_n)$ acc. to AGMA 1102-A03 [23] (Table 2)							

5.2. Definition of reference geometries and variables considered

The investigation was carried out on the basis of a reference hub geometry, which was chosen as a representative case for the scope of this research: small and highly crowned geometry suitable for a high misalignment angle application. In this study, a total of 11,480 geometries were generated.

The range of values selected together with the reference value for each design variable were determined in regards to the following considerations and are shown in Table 4 (underlined values correspond to the reference values):

- Number of teeth, z or associated module m_n.
  No reference value was selected.
  Range: 0.5-10, taken from the standard ISO 4156 [17], where a minimum of 6 teeth and a maximum of 100 is recommended.

- Crowning ratio, ε.
  No reference value was selected.
  Range: $\varepsilon \leq 1.0$, as they are special cases in the existing literature [22, 25], and have not been previously studied. In this analysis crowning ratios below this limit were chosen, with the minimum mathematical limit of $\varepsilon = 0.4$.

- Pressure angle, α.
  Reference value: 30°, because it is the most used in gear coupling applications [16, 20, 22].
  Range: defined from the standard ISO 4156 [17], and additionally a 20° pressure angle was considered, as it is a reference in load capacity calculations of gears and is also one of the most used in gear couplings [22].

- Aspect ratio, b/d_p.
  Reference value: 0.30, as it is suggested for gear couplings working in high misalignment angle applications in the specialized literature [22, 32, 33].
  Range: selected in accordance to literature recommendations: $b/d_p = 0.15$, for the purpose of comparison; $b/d_p = 0.60$, reference value for the standard DIN 5466 [20]; and, $b/d_p = 0.90$, since it is recommended that the length must be less than the gear pitch diameter to prevent torsional twist concentrations in external gears [34].

- Pitch diameter, d_p.
  Reference value: 50 mm, for being an appropriate size for the current analysis.
  Range: 36-400 mm, so that a wide range of sizes is covered, and general conclusions can be drawn.

- Clearance factor, k
  Reference value: 0.07, since it is the highest value from the range recommended [22], and a bigger clearance will enable a higher misalignment angle.
  Range: 0.04-0.08, to analyze a wider range than the one recommended in literature [22], which at the same time, gives no guidelines to choose an appropriate value.

Table 4: Definition of the design variables for the research case studies.

Parameter	Values considered
m_n [mm]	0.5, 1.0, 1.5, 2.0, 3.0, 4.0, 5.0, 6.0, 8.0, 10.0
ε [-]	0.4, 0.5, 0.6, 0.7, 0.8, 0.9, 1.0
α [°]	20, <u>30</u>, 37.5, 45
b/d_p [-]	0.15, <u>0.30</u>, 0.60, 0.90
d_p [mm]	36, <u>50</u>, 100, 200, 400
k [-]	0.04, 0.05, 0.06, <u>0.07</u>, 0.08

Additionally, to generate these geometries a circular tool path was used, as it is the most commonly used in gear couplings [5, 11, 27]. Here, the tool path radius r_β was defined based on the crowning ratio ε, the pitch radius r_p and the hob pitch radius r_{pw} (see Fig. 3(a)), as:

$$r_\beta = \varepsilon \cdot r_p + r_{pw} \tag{24}$$

In all the cases, a spherical gear blank was employed to generate the different geometries, with an external radius equivalent to the tip radius of the hub. This geometry was selected to prevent interference in misaligned applications when rotating relative to the pivoting position of the gear coupling [35].

6. Results

The geometries were generated following the model described in Section 2. The geometrical properties were verified according to the conditions of existence in Section 4, and the achievable maximum misalignment was calculated with the proposed algorithm in Section 3.2.

In the following sections the effect of the design parameters on the maximum misalignment angle and geometry characteristics is analyzed.

6.1. Maximum misalignment angle: literature comparison

First, the misalignment value obtained with equations (10, 11) from the literature was compared with the model proposed in Section 3.2. To this end, the equations were applied to gear coupling geometries from the literature (**L**) and some representative case studies (**CS**) to determine the maximum misalignment angle. All the geometry properties are summarized in Table 3.

Figure 7 shows the results of the models ordered from the highest to the lowest crowning ratio value ε, together with the geometry generated by the model summarized in Section 2.

The straight gear coupling **L1** has the highest ε value, with an infinite crowning radius. It can be seen that there is disparity between the results obtained with the different equations. Indeed, due to the infinite value of the crowning radius r_c, the equations give a null misalignment angle. By contrast, the proposed model gives a $\gamma \approx 0.2°$ due to the consideration of the tooth geometry and the existing clearance in the gear coupling. Even though, this would not be an appropriate working angle due to the stress concentration resulting from edge contact [29]. Thus, it can be said that the equations are not suitable to analyze straight gear couplings with a an infinite crowning radius r_c.

In the case of **L2**, **L3** and **L4** geometries, all equations present similar results. These geometries have a high value crowning radius r_c, and thus a small amount of longitudinal crowning $C_{h\beta}$. Moreover, it can be seen that the pitch diameter does not have a significant effect on the results for cases **L2** and **L3**. However, differences can be perceived with eqn. (11) in **L4**, which is a relatively small gear coupling with a low crowning ratio.

This observation is reinforced by the results obtained with **CS1** and **CS2**, where it can be seen that for relatively small pitch diameters and $\varepsilon = 1.0$ the values obtained with eqn. (11) differ to a greater extent.

The lowest ε value in this analysis corresponds to the case studies **CS3** and **CS4**, where deviations are more noticeable. Differences with eqn. (11) are even greater than for the previous cases, due to the lower crowning ratios. Indeed, a lower crowning ratio (ε) means a smaller crowning radius (r_c) and thus, a higher amount of crowning ($C_{h\beta}$).

The figure clearly shows that eqn. (10), gives similar results to the proposed model for the literature cases (**L1**, **L2**, **L3**, **L4**) and the case studies with a high crowning ratio (**CS1**, **CS2**). However, for the case studies with a smaller crowning ratio (**CS3**, **CS4**) differences increase. The deviations are particularly visible in **CS3**, where due to the

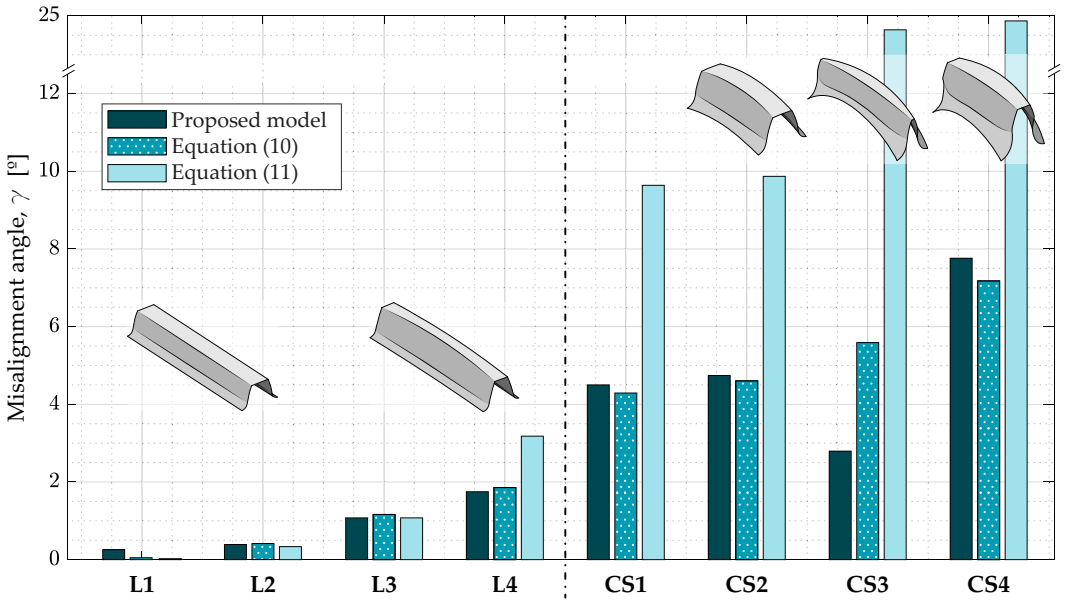

Figure 7: Maximum misalignment angle calculated according to the literature and the proposed model applied to the geometries defined in Table 3.

bigger pitch diameter, the face width of the hub is increased to keep a constant aspect ratio. This feature causes the maximum misalignment angle to decrease, which is not considered in eqn. (10).

Hence, it is shown that either the crowning ratio or the pitch diameter have an impact on the calculated misalignment angle value. This demonstrates the need for a more in-depth analysis to determine the influence of gear coupling design variables, which is developed in the subsequent sections.

6.2. Influence of the module and number of teeth

To analyze the influence of the design variables in terms of the number of teeth z and the crowning ratio ε, every geometry for each number of teeth and crowning ratio was generated for the corresponding pitch diameter.

In this case the analyzed geometries were generated with the following parameters:

- Constant parameters: $d_p = 50$ mm, $\alpha = 30°$, $b/d_p = 0.3$, and $k = 0.07$.
- Variable parameters: m_n and ε.

Figure 8 shows the maximum misalignment angle achieved with each of the hub geometries generated according to Table 4. Black points in Fig. 8, illustrate the geometries obtained with the reference value of $\varepsilon = 0.4$, while the rest of the points with a constant number of teeth represent the geometries generated with the same parameters, but a different crowning ratio value.

It can be seen that the maximum misalignment angle decreases for a constant pitch diameter as the number of teeth increases (or module decreases), regardless of the crowning ratio. However, the crowning ratio has a higher influence on geometries with low numbers of teeth. The maximum misalignment angle ($\gamma_{\max} = 11.5°$) may be reached with a $z = 6$ and $\varepsilon = 0.4$ hub geometry. Moreover, the maximum variation observed due to the change in the number of teeth is of $\Delta\gamma = 9.19°$, which corresponds to an effect of 79.91%.

Moreover, the figure shows two areas, corresponding to the geometries that do and do not verify the conditions of existence, proposed in Section 4. Each region is delimited by a convex hull, which refers to the smallest convex polygon that includes all the points in a 2D space. Here, this is determined by Andrew's monotone chain convex hull algorithm [36].

A representative hub tooth geometry corresponding to each of the zones can be seen on the right side of Fig 8. The zone that fulfills the conditions of existence (so-called *Verified*) covers the lower part of the graph (striped zone),

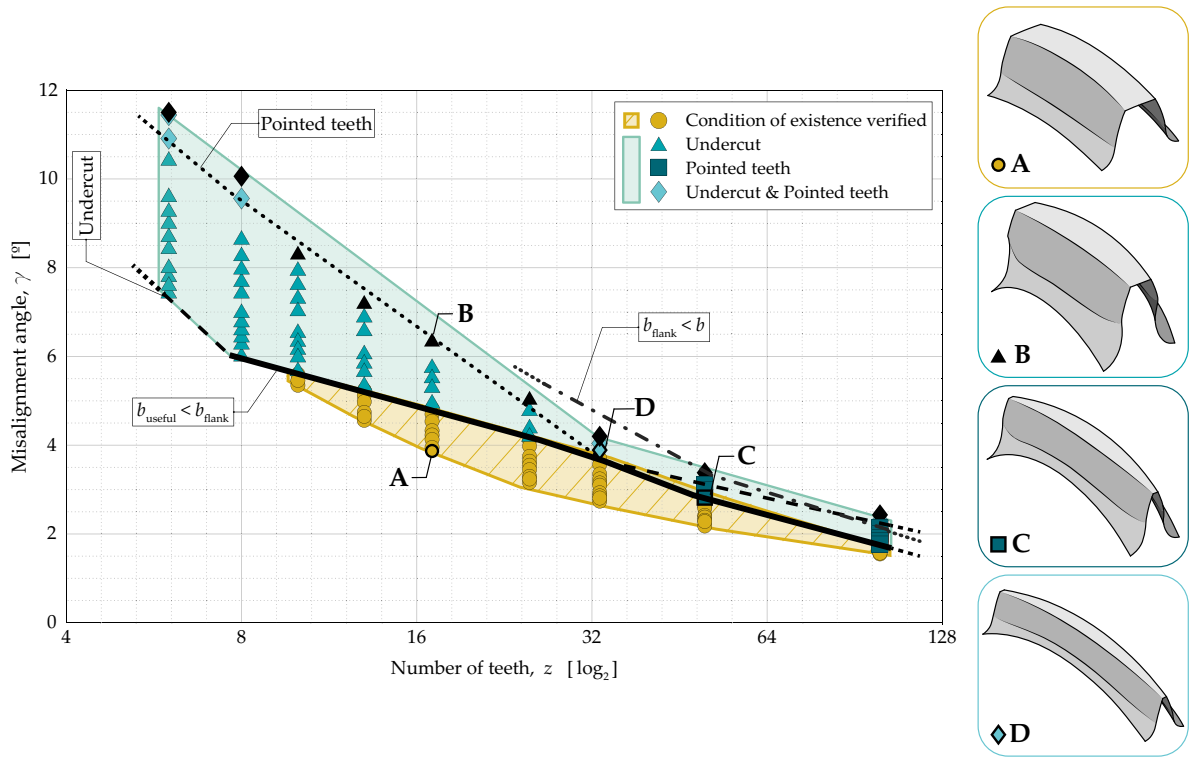

Figure 8: Maximum misalignment angle for $d_p = 50$ mm, $\alpha = 30°$, and $b/d_p = 0.3$ geometries (black symbols for $\varepsilon = 0.4$) and geometrical boundaries in terms of the number of teeth z: Dashed line $(--)$ for undercut, dotted line $(\cdot\cdot)$ for pointed teeth, and dashed and dotted line $(-\cdot)$ for flank length shorter than the face width.

where the smallest misalignment angles are achieved. The hub geometries in this zone do not have any undercut sections nor pointed teeth issues. It should also be noted that this area can be further extended to lower misalignment values with higher crowning ratios ($\varepsilon > 1.0$), however these common geometries are out of the scope of this research.

On the left of the figure, where the highest misalignment angles are achieved, undercut sections (▲) prevail. Moreover, if a misalignment angle above 6° is required, undercut sections will be unavoidable, and thus it is necessary to generate and control the geometry of the undercut sections properly by using the tooth generation procedure described in [12].

Concerning the pointed teeth zone (■), the figure shows that it appears in geometries with higher numbers of teeth. It can also be found, in small numbers of teeth for very high misalignment angles, which require large longitudinal crowning.

Finally, with regard to the useful flank, Fig. 8 depicts the limit (straight and thick line) at which the useful flank length is smaller than the flank length (which is equal to the face width of the hub). This limit coincides with the lower limit at which undercut and pointed teeth start, confirming that the geometries inside the *Verified* region are the most appropriate from the point of view of stiffness or larger contact surface (the aspect ratio is equivalent to the useful flank ratio). Indeed, once the hub geometry presents singularities, the length of the useful profile b_{useful} starts to decrease. In cases with a large number of teeth, the limiting line that defines the misalignment angle from which the flank length is smaller than the face width hub ($b_{\text{flank}} < b$) is denoted with a dashed and dotted line. The geometries above this boundary are the ones with the smallest useful flank ratios.

6.3. Influence of the crowning ratio ε

The geometries analyzed herein were generated with the same parameters from the precedent section:

- Constant parameters: $d_p = 50$ mm, $\alpha = 30°$, $b/d_p = 0.3$, and $k = 0.07$.

- Variable parameters: m_n and ε.

Related to the results presented above, Fig. 9 shows the influence of the crowning ratio on the maximum misalignment angle. In addition to the maximum misalignment angle represented with the contour plot, the hub geometries in each zone of the figure are also displayed to graphically illustrate the influence of the design variables on the generated tooth geometry.

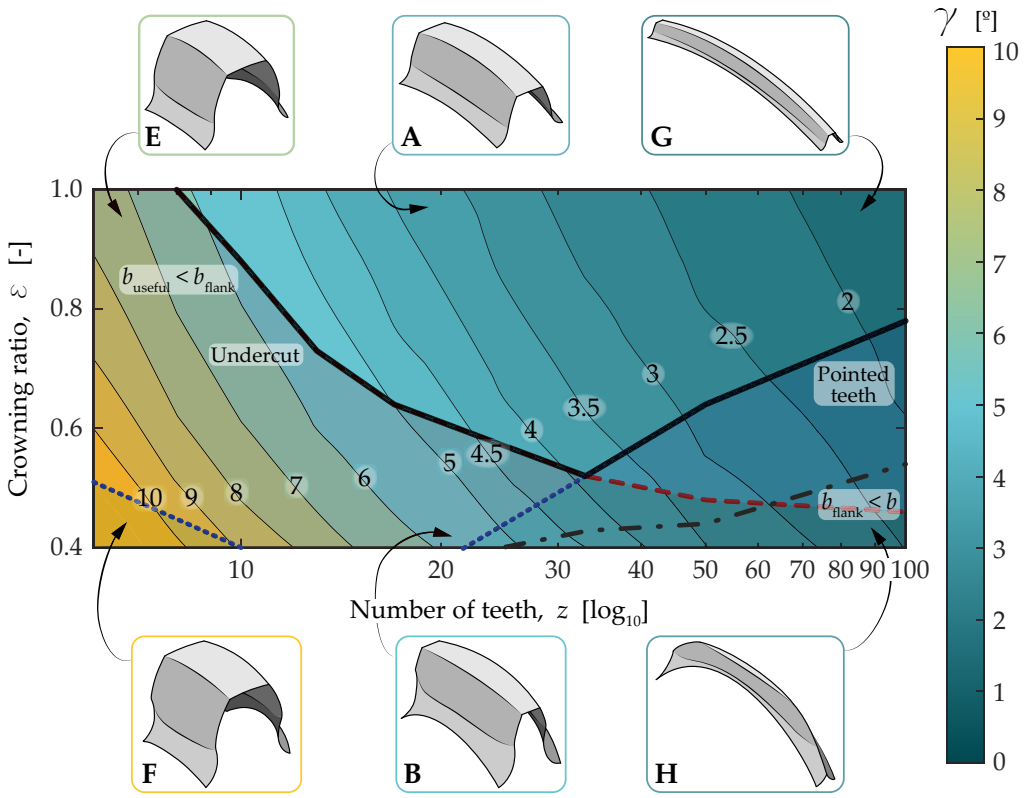

Figure 9: Maximum misalignment angle in terms of the crowning ratio and the number of teeth for $d_p = 50$ mm, $\alpha = 30°$, and $b/d_p = 0.3$ geometries. Dashed line (– –) represent the undercut condition, while the dotted line (· ·) the pointed teeth, and the dashed and dotted line (– ·) the limit where the flank length is shorter than the face width.

It can be seen that as the number of teeth and the crowning ratio increases, the maximum misalignment angle decreases. Even if a decrease of the crowning ratio presents a direct increase of the misalignment angle, it will not increase with the same amount for all geometries. Moreover, the misalignment angle evolution decreases as the number of teeth increases, for the same crowning ratio variation. For instance, a decrease from $\varepsilon = 1.0$ (geometry **E**) to $\varepsilon = 0.4$ (geometry **F**) of two geometries with $z = 6$, results in an increase of the maximum misalignment angle of $\Delta\gamma = 4.03°$. However, for the same pitch diameter in two geometries with $z = 100$ (**G** and **H**), the same crowning ratio variation ($\Delta\varepsilon = 0.6$) only produces an increase of the misalignment angle of $\Delta\gamma = 0.86°$. The maximum variation observed due to the change in the crowning ratio is of $\Delta\gamma = 4.03°$, which corresponds to an effect of 35.04%.

The conditions of existence are represented in Fig. 9 with the undercut boundary as a dashed line, and the pointed teeth boundary as a dotted line. The small number of teeth (high module) geometries are more likely to have undercutting sections, while geometries with a higher number of teeth (small module) present pointed teeth. This result is consistent with the gear literature [37]. Furthermore, these results clearly show that to achieve a high misalignment angle the presence of undercut is mandatory.

Concerning the flank length, the geometries inside the non-shaded region (e.g. geometries **A** and **G**) contain hubs with a useful flank b_{useful} equivalent to the flank length b_{flank} and face width b of the hub. Below this boundary, the useful flank is shorter than the flank length. For smaller crowning ratios and at high numbers of teeth, with a dashed

and dotted line, the flank length is shorter than the face width (e.g. geometry **H**), thus more flexible geometries are obtained.

6.4. Influence of the pressure angle α

Here, geometries were generated with the corresponding parameters:

- Constant parameters: $d_p = 50$ mm, $b/d_p = 0.3$, and $k = 0.07$.
- Variable parameters: α, m_n and ε.

Figure 10 depicts the influence of the pressure angle on the maximum misalignment angle. The four graphs in the figure represent the maximum misalignment angle for each pressure angle in terms of the number of teeth, and a representation of $\mathbf{B}_x$ geometry is also depicted.

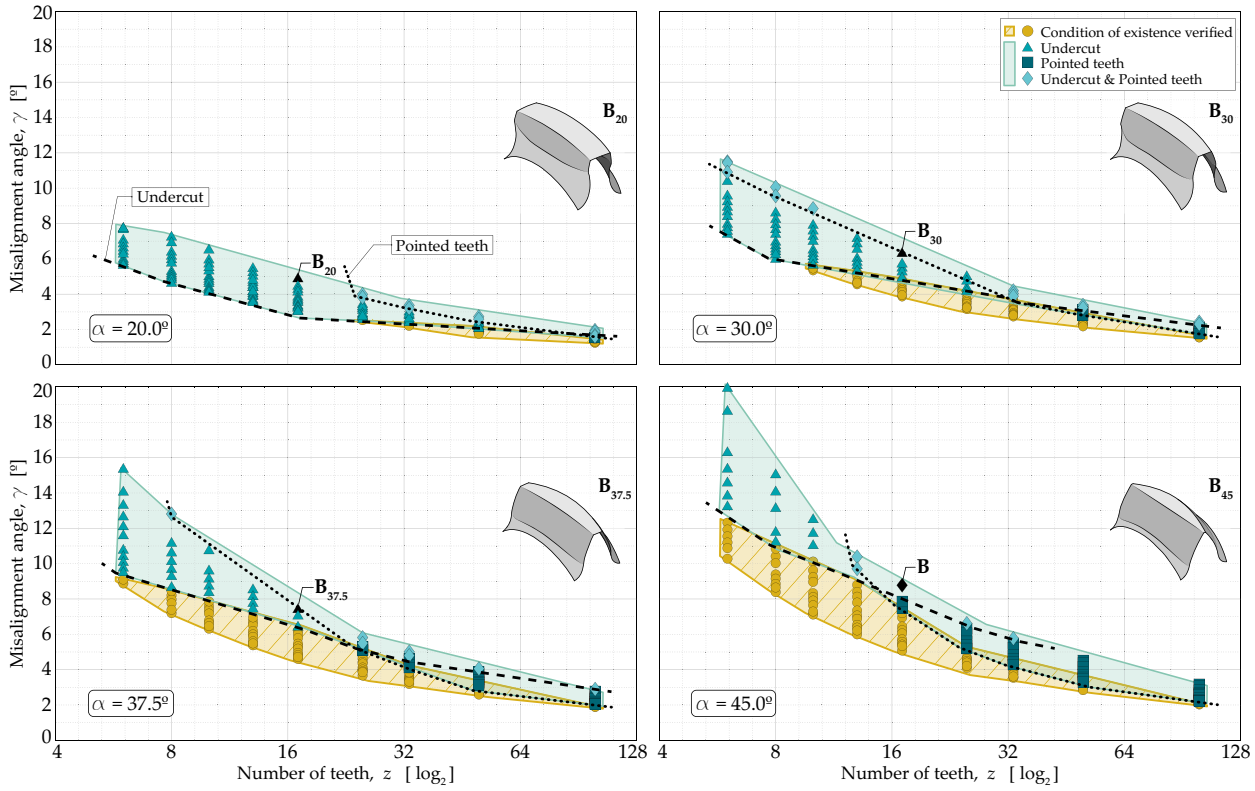

Figure 10: Maximum misalignment angle for different pressure angles for $d_p = 50$ mm and $b/d_p = 0.3$ geometries. Dashed line $(--)$ represent the undercut condition, while the dotted line $(\cdots)$ the pointed teeth limit.

Figure 10 shows a decrease of the maximum misalignment angle as the number of teeth increases, regardless of the pressure angle. Moreover, it can be observed that for the same geometry with the same parameters, the achievable maximum misalignment angle increases as the pressure angle increases. For instance, geometry $\mathbf{B_{20}}$ attains a maximum misalignment of $\gamma = 4.95°$ for $\alpha = 20°$, while it increases up to $\gamma = 8.78°$ in geometry $\mathbf{B_{45}}$ for $\alpha = 45°$. Furthermore, the influence of the number of teeth increases as the pressure angle increases; i.e. for a geometry of $\alpha = 20°$ and $\varepsilon = 0.4$, a change of the number of teeth can vary the maximum misalignment angle as much as $\Delta\gamma = 5.84°$, whereas for a $\alpha = 45°$ and $\varepsilon = 0.4$, it may vary up to $\Delta\gamma = 15.53°$. The maximum misalignment angle ($\gamma_{\max} = 20.36°$) may be reached with a $z = 6$ and $\alpha = 45°$ hub geometry. Moreover, the maximum variation observed due to the change in the pressure angle is of $\Delta\gamma = 12.56°$, which corresponds to an effect of 61.69%.

Concerning the conditions of existence, the results show that as the pressure angle increases the pointed teeth region increases, while the undercutting region is reduced to small number of teeth geometries.

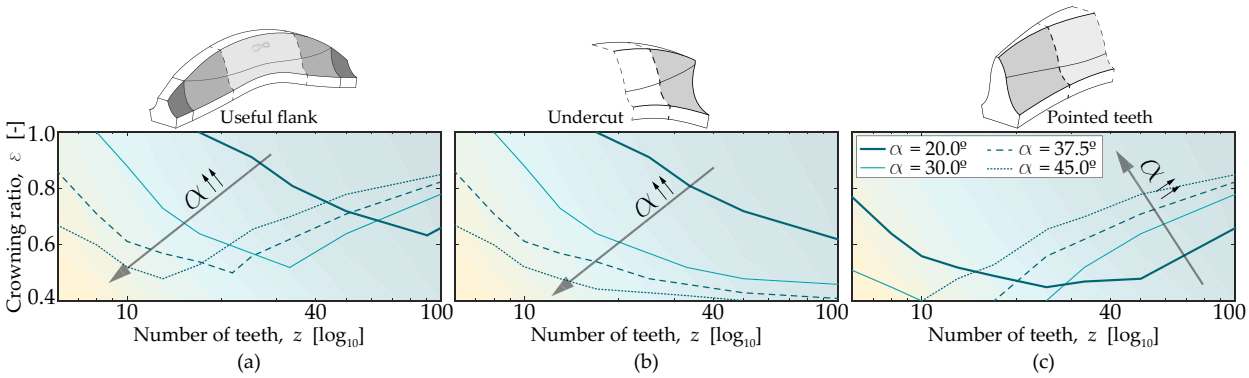

Figure 11: Conditions of existence for $d_p = 50$ mm and $b/d_p = 0.3$ geometries in terms of the pressure angle: (a) useful flank, (b) undercut, and (c) pointed teeth.

It should also be noted, that if very high misalignment angles need to be achieved undercutting is necessary, for all pressure angles. Nevertheless, for high misalignment angles between 3-10° it can be seen that geometries with low numbers of teeth and a large pressure angle (37.5° or 45°) can prevent undercut sections.

Figure 11 illustrates the useful flank, undercut and pointed teeth limits in terms of the crowning ratio and number of teeth. Figure 11(a) shows how the useful flank region increases towards the bottom left corner, as the pressure angle increases, making it clear that a higher pressure angle with low number of teeth provide a more suitable gear hub from the geometrical point of view. Figure 11(b) and (c) present similar trends: the undercut region is reduced when the pressure angle increases, and at the same time, the pointed teeth area is enlarged when the pressure angle increases.

6.5. Influence of the aspect ratio b/d_p

To analyze the influence of the varying face width, these geometry parameters were used:

- Constant parameters: $d_p = 50$ mm, $\alpha = 30°$, and $k = 0.07$.
- Variable parameters: b/d_p, m_n and ε.

Figure 12 shows the maximum misalignment in terms of the number of teeth, together with the representation of the geometry $\mathbf{B}_x$ according to the aspect ratio. It can be seen, that an enlargement of the face width does not affect the achievable misalignment angle, except for small numerical deviations, even though there is a severe increase of the pointed teeth region. The maximum variation observed due to the change in the aspect ratio is of $\Delta\gamma = 0.05°$, which corresponds to an effect of only 0.56%.

Figure 13 depicts that a value of the aspect ratio $b/d_p > 0.6$ adversely affects the geometrical properties in small pitch diameters, due to the excessive pointed teeth. Moreover, no apparent increase in the misalignment angle is observed.

Concerning lower aspect ratio values ($b/d_p = 0.15 - 0.3$), a stress analysis is required, as the achievable misalignment angle will remain constant for small pitch diameter geometries.

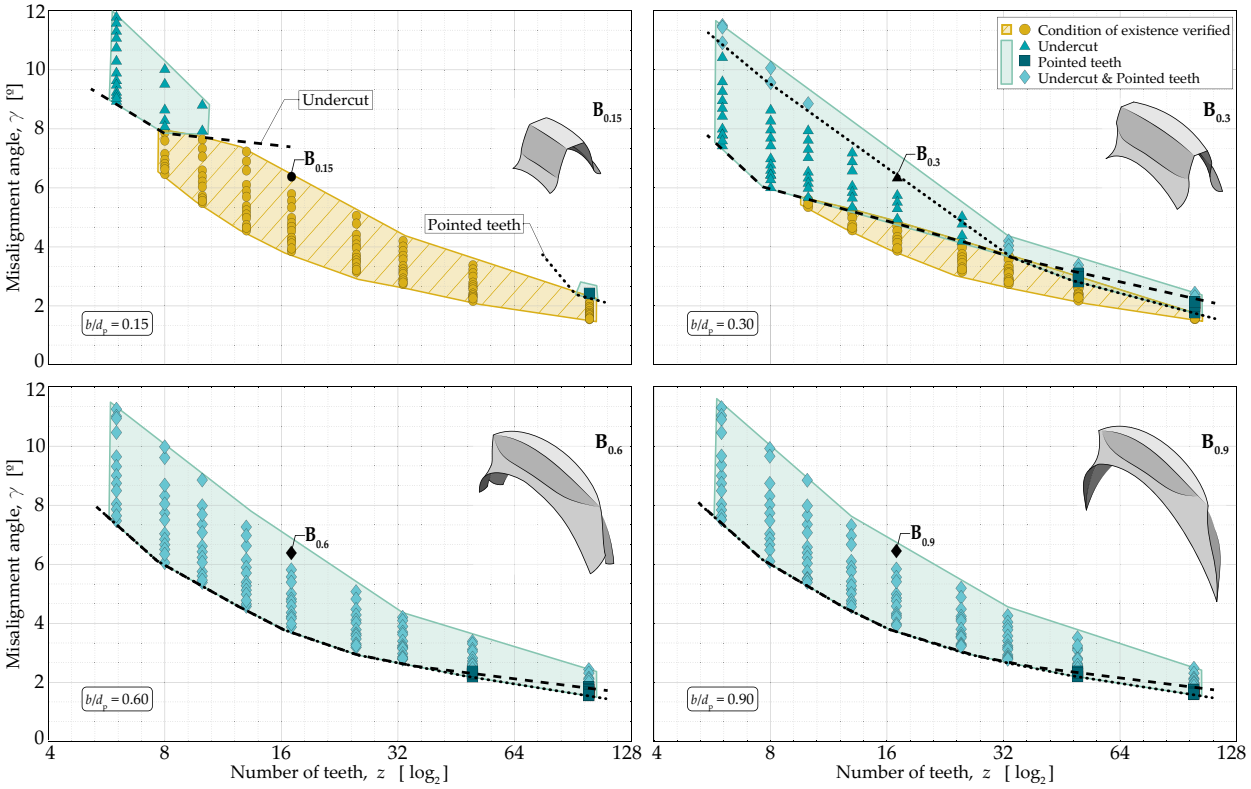

Figure 12: Maximum misalignment angle for different aspect ratios in $d_p = 50$ mm and $\alpha = 30°$ geometries. Dashed line $(--)$ represent the undercut condition, while the dotted line $(\cdot\cdot)$ the pointed teeth limit.

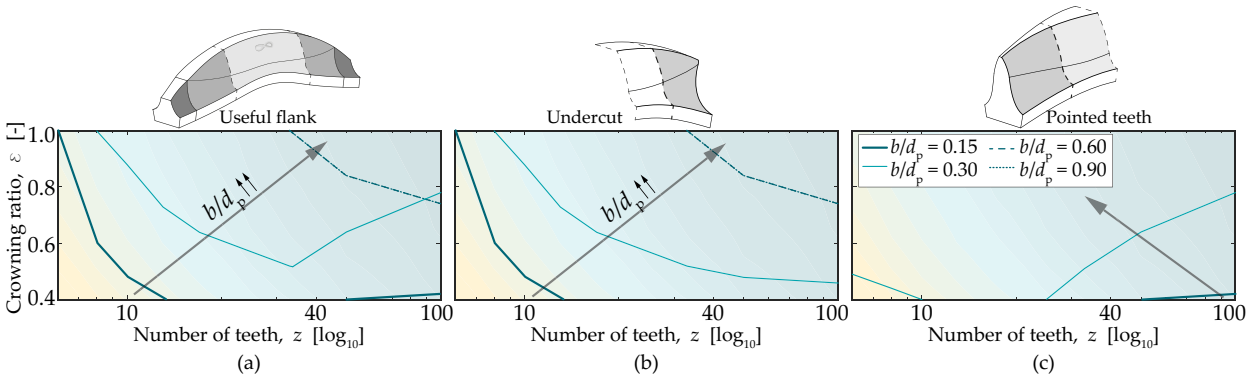

Figure 13: Conditions of existence for $d_p = 50$ mm and $\alpha = 30°$ in terms of the aspect ratio: (a) useful flank, (b) undercut, and (c) pointed teeth.

6.6. Influence of the pitch diameter d_p

To this point, the influence of the design variables has been analyzed considering a constant space constraint, that is, a constant pitch diameter of $d_p = 50$ mm. In this section the impact of the pitch diameter is described and geometry parameters were set as follows:

- Constant parameters: $\alpha = 30°$, $b/d_p = 0.3$, and $k = 0.07$.
- Variable parameters: d_p, m_n and ε.

Figure 14(a) shows a general overview of the maximum misalignment angle achieved with all the generated

geometries, in terms of the pitch diameter and the number of teeth.

It can be observed that the highest misalignment angles are achieved with small pitch diameters ($d_p < 100$ mm), regardless of the crowning ratio used. In other words, as the pitch diameter increases the maximum misalignment angle decreases (Fig. 14(b)). In addition, the variation of the obtained maximum misalignment angle is smaller as the pitch diameter increases. The figure also illustrates the decrease of the achievable maximum misalignment angle while the number of teeth increases, with a common limiting surface, regardless of the pitch diameter.

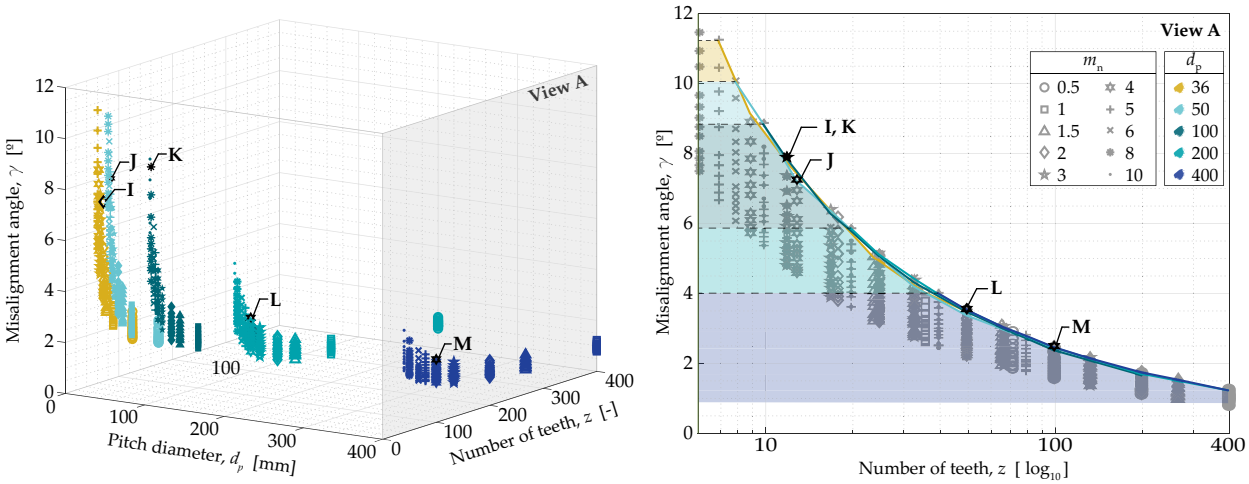

Figure 14: (a) Maximum misalignment angle under different pitch diameter and numbers of teeth for $\alpha = 30°$ and $b/d_p = 0.3$ geometries. (b) Maximum misalignment angle achieved in terms of the number of teeth for each pitch diameter. (For color legend interpretation, the reader is referred to the web version of the article.)

For a constant number of teeth and crowning ratio, the maximum misalignment angle achieved is very similar, regardless of the pitch diameter. For instance, for geometries **I** ($z = 12$), **J** ($z = 13$) and **K** ($z = 12$), and $\varepsilon = 0.4$, and the maximum misalignment angle is 7.87°, 7.23° and 7.91°, respectively (see Fig. 15). These slight differences are associated with the different number of teeth, due to the predefined module values in the ISO 4156 standard [17]. The maximum variation observed due to the change in the pitch diameter by the module is of $\Delta\gamma = 0.98°$, which corresponds to an effect of 7.80%.

Similarly, if the same module and crowning ratio geometries are compared for different pitch diameter values, a significant decrease of the maximum misalignment angle is observed; e.g. for geometries **J**, **L** and **M** with $m_n = 4$ mm and $\varepsilon = 0.4$, a maximum misalignment angle of 7.23°, 3.53° and 2.47° is achieved, respectively. The maximum variation observed due to the change in the pitch diameter by the number of teeth is of $\Delta\gamma = 6.57°$, which corresponds to an effect of 73.99%. It can therefore be concluded, that although the module and the number of teeth are variables dependent on each other ($d_p = m_n\, z$), the number of teeth z has a greater impact on the achievable maximum misalignment angle.

Indeed, within the recommended module and number of teeth values from ISO 4156 [17], it can be observed that as the pitch diameter increases, the available area is reduced (geometries outside the boundaries are shaded: $z < 6$ and $z > 100$). The misalignment angle differences within this area are thus reduced, and a geometry that verifies the conditions of existence is easier to obtain. Nevertheless, if the design demands a high misalignment angle, from Fig. 15 it can be deduced that geometries with a small pitch diameter and low number of teeth are the most suitable, even if undercut singularities exist.

To clearly state the limiting values of the crowning ratio at which conditions of existence are fulfilled, Fig. 16 shows the similarity of the boundaries for the useful flank (a), undercut (b) and pointed teeth (c) for all the pitch diameters. The slight differences are related to the numerical deviations. In fact, it is evidenced that the crowning ratio has no influence on the pitch diameter.

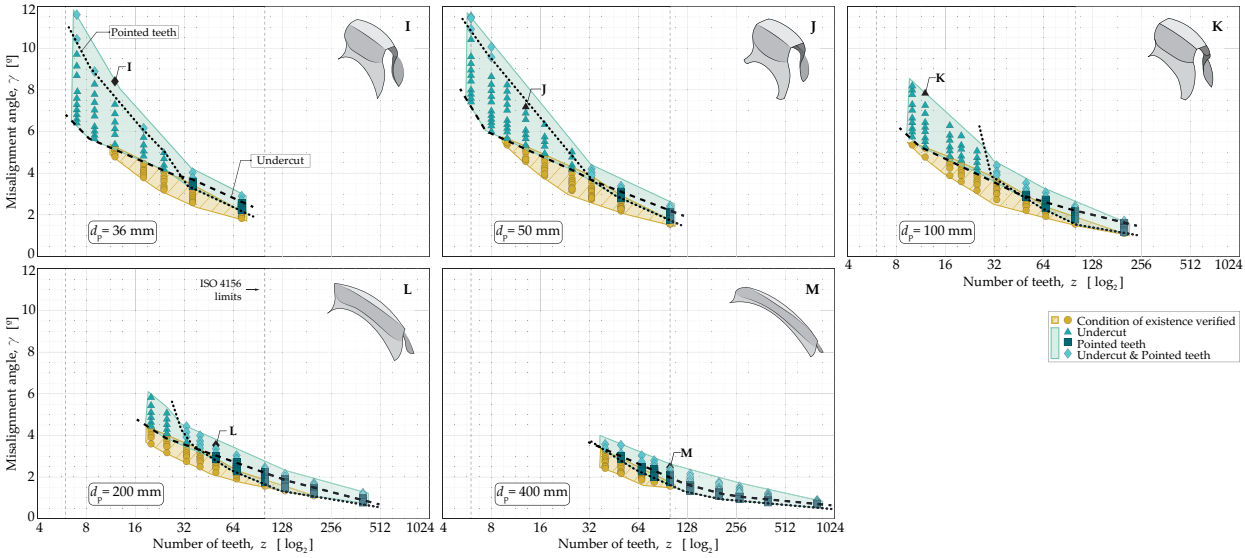

Figure 15: Maximum misalignment angle for $\alpha = 30°$ and $b/d_p = 0.3$ geometries for each pitch diameter. Dashed line $(- -)$ represent the undercut condition, while the dotted line $(\cdot\cdot)$ the pointed teeth limit.

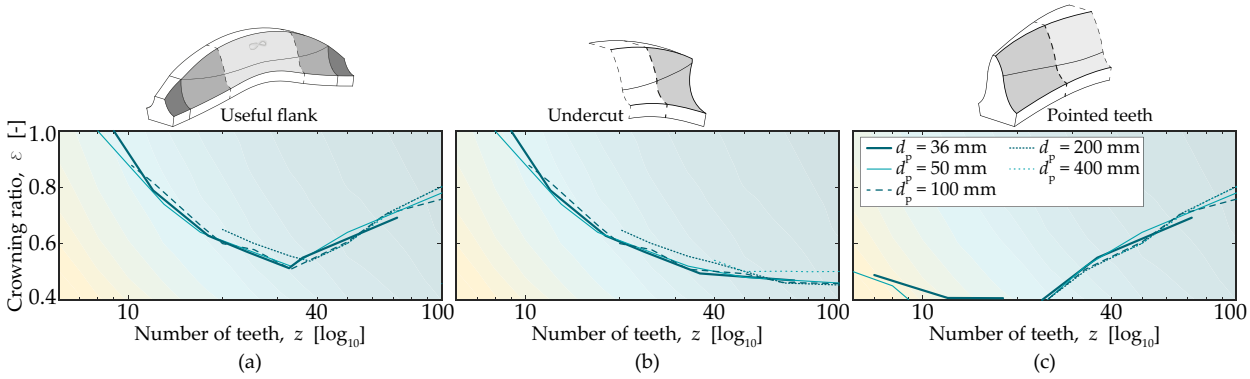

Figure 16: Conditions of existence for $\alpha = 30°$ and $b/d_p = 0.3$ geometries in terms of the pitch diameter. (a) useful flank, (b) undercut, and (c) pointed teeth.

6.7. Influence of the clearance factor k

Finally, the influence of the clearance between the hub and the sleeve tooth surfaces was analyzed, using the clearance factor k, and with the subsequent parameters:

- Constant parameters: $d_p = 50$ mm, $\varepsilon = 0.4$, $\alpha = 30°$, and $b/d_p = 0.3$.
- Variable parameters: k and m_n.

Even if clearance distribution changes as a function of the teeth angular position or due to manufacturing errors [38, 16], attention was paid to the minimum clearance value in the tilting position (see Fig. 17), to analyze its effect on the misalignment angle.

Figure 17 shows the increase of the misalignment angle as the clearance factor k increases, in terms of the number of teeth.

The clearance value ($j = k \cdot m_n$) is in terms of the module, and thus for a constant pitch diameter, a smaller number of teeth will have a greater clearance value. This is also consistent with the observation that the influence of the clearance factor is more marked in geometries with a small number of teeth. Hence, if a $z = 6$ and $z = 100$ are compared, the misalignment variation reduces from $\Delta\gamma = 2.30°$ to $\Delta\gamma = 0.83°$ in terms of the clearance factor k.

The maximum variation observed due to the change in the clearance factor is of $\Delta\gamma = 2.30°$, which corresponds to an effect of 18.70%.

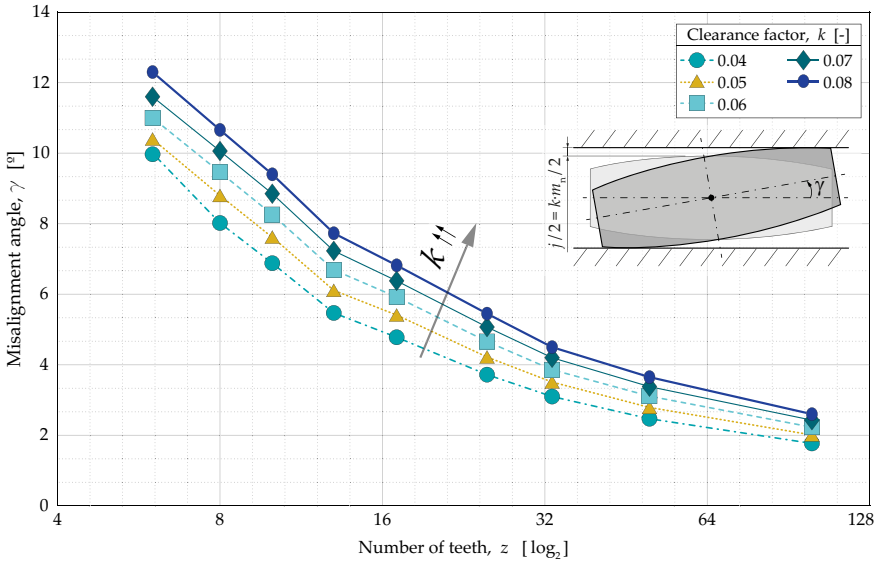

Figure 17: Misalignment angle in terms of the clearance factor k for $d_p = 50$ mm, $\alpha = 30°$ and $b/d_p = 0.3$, and representation of misalignment angle variation.

7. Discussion

In accordance with the analytical models in the literature proposed in equations (10, 11) to determine the misalignment angle, it has been shown that deviations arise for small crowning ratios or big face width gear couplings, as these are oriented for small misalignment angles. Indeed, these equations do not consider all the parameters involved or the real geometry of the hub tooth, such as the face width, the module or the clearance. Related to this, in eqn. (11) simplifications associated with the transverse crowning radius r_t calculation are made. Indeed, in (11) the transverse crowning radius is approximated as: $r_t = r_c \cdot \tan(\alpha)^{-1}$, but this equivalence is only satisfied when the transverse crowning radius r_t is large enough (big crowning ratios), and the contact point is in the pitch diameter.

From the parameters analyzed in this paper it can be concluded that geometries with low numbers of teeth are the most suitable to attain higher misalignment angles, even if they are susceptible to undercut singularities. This is in agreement with the design criteria proposed by Herbstritt and Paluh [19]. They found that larger and fewer teeth with a small curvature (r_c) result in significant stress reduction and increased life of the component, which makes them more suitable for high misalignment applications [38]. In the same vein, Section 6.6 shows that small pitch diameters provide the largest design space for high misalignment angles.

Concerning the design variables, the present paper has shown that crowning radius is a key parameter in the design of highly misaligned hubs. Similarly, some works have noted that longitudinal crowning is necessary to compensate for misalignment [3, 16]. Moreover, it is said that an excessive longitudinal crowning (reduced crowning radius) leads to uneven clearance distribution [3]. This can also be observed in Fig. 8 and 9, by the fact that a geometry optimized for a higher misalignment angle than the angle it is working at, will have bigger undercut singularities, and thus a lower stiffness. The aforementioned issue is dependent on the useful flank, as crowning ratio is reduced, the useful flank is also reduced. However, if crowning ratio is kept constant and the face width of the gear coupling varies, neither the misalignment angle nor the useful flank values change significantly, due to the small value crowning radius r_c existing in these geometries. This appears to be in agreement with Dudley [39], who stated that in flexible gear couplings the face width does not necessarily contribute to load-carrying capacity, and concluded that increasing the face width will not increase the load capacity. In fact, in Fig. 12 it is observed that there is a limit b/d_p ratio above

which the maximum misalignment angle does not vary. AGMA 945-1-B20 [16] also stated that a face width limit exists, above which root stresses are not reduced. Hence, it can be concluded that the most suitable aspect ratio values are $0.15 < b/d_p < 0.3$, which is in agreement with recommended values from the literature [22, 32, 33], even if these latter were never verified for such big misalignment angles.

On the other hand, the standard pressure angles commonly applied in the literature are 20° [3, 22] or 30° [17, 20]. Nevertheless, the present work demonstrates that large pressure angles (45°) offer the best geometry adapted to high misalignment applications. Indeed, a higher pressure angle will generate a wider tooth root and ultimately a stiffer tooth. Alfares et al. [3] sets a minimum pressure angle of 25° for high misalignment applications, even if wear problems arise with values higher than 40°. The discrepancy with the proposed suitable pressure angle of 45° in the present paper, might be due to the non extended use of gear couplings in high misalignment applications. Moreover, wear failures are common in slight misalignment applications [40], and there are no evidence of wear failures in high misalignment applications.

Finally, concerning the clearance, standards [17, 20] recommend increasing the clearance values when misalignment occurs, but no guide values are provided. This work has shown that an increase of the clearance value does in fact increase the maximum misalignment angle. However, it is known that smaller clearance values lead to increased uniformity of tooth loading [3, 38], while higher values generate less uniform load distributions [41]. There are some works that propose clearance values depending on the pitch diameter [39] or module [22], but they are not adapted to working operations at high misalignment angles.

8. Conclusions

In this work, an algorithm to calculate the maximum misalignment angle is proposed, which considers real gear coupling teeth geometries and all the design parameters involved in the misalignment angle calculation. After comparing the results with other models in the literature, it is concluded that:

(1) The proposed model, can be applied for all type of gear coupling geometries, and it is not limited to gear couplings with small amounts of crowning ($\ll 100 \cdot 10^{-3}$ mm), as is the case with existing methods.

(2) The transverse crowning radius cannot be approximated to the crowning radius by $r_t = r_c/\tan(\alpha)$, in highly crowned spherical gear couplings.

(3) The face width and the module must be considered when calculating the maximum misalignment angle, together with the crowning radius, the pressure angle, and the clearance.

Secondly, the influence of the main design parameters of spherical gear couplings on the geometrical properties of gear tooth surfaces that work in high misalignment applications was investigated. These analyses allow the following conclusions to be drawn:

(4) The proposed procedure to define the limits of the main design parameter for spherical gear couplings is effective to prevent tip pointing and undercutting profiles in highly crowned spherical gear couplings.

(5) Gear couplings adapted to high misalignment angles ($\gamma > 5°$) must have undercutting profiles, which in consequence need to be accurately generated with an appropriate model.

(6) The maximum effect of each design parameter on the maximum misalignment angle individually are, from highest to lowest: the number of teeth (79.91%), the pressure angle (61.69%), the crowning ratio (35.04%), the clearance factor (18.70%), and the pitch diameter (7.80%). The aspect ratio, has no significant influence on small geometries (0.55%), with the most appropriate value being $0.15 < b/d_p < 0.3$.

(7) High pressure angle geometries give rise to hub tooth surfaces with verified geometric tooth surfaces at high misalignment angles.

This work serves as a tool for designers and manufacturers to choose the most appropriate highly crowned spherical gear coupling geometry adapted to a required maximum misalignment angle.

This design space will require future validation with a stress analysis. Indeed, in load conditions, the number of teeth in contact will vary in the presence of high misalignment and thus, flexibility of the gear coupling will be modified giving as a result slightly larger misalignment angles.

References

[1] S. Hahn, Coupling Connections and Splines, in: Encyclopedia of Automotive Engineering, John Wiley & Sons, 2014, pp. 1–14. doi:10.1002/9781118354179.auto094.

[2] Y. Guo, S. Lambert, R. Wallen, R. Errichello, J. Keller, Theoretical and experimental study on gear-coupling contact and loads considering misalignment, torque and friction influences, Mechanism and Machine Theory 98 (2016) 242–262. doi:10.1016/j.mechmachtheory.2015.11.015.

[3] M. Alfares, A. Falah, A. Elkholy, Clearance distribution of misaligned gear coupling teeth considering crowning and geometry variations, Mechanism and Machine Theory 41 (10) (2006) 1258–1272. doi:10.1016/j.mechmachtheory.2005.11.004.

[4] F. Ohshima, S. Hirata, H. Yoshino, Study on Tooth Contact of Gear Couplings, Transactions of the Japan society of mechanical engineers. Series C 78 (786) (2012) 639–649. doi:10.1299/kikaic.78.639.

[5] Y. Guan, X. Yang, Z. Fang, G. Chen, Comparative analysis of three geometric models for crown gear coupling, Mechanism and Machine Theory 136 (2019) 269–283. doi:10.1016/j.mechmachtheory.2019.02.016.

[6] J. R. Mancuso, Couplings and joints: design, selection and application, Technology & Engineering. M. Dekker, 1986.

[7] P. Krot, Transient torsional vibrations control in the geared drive trains of the hot rolling mills, in: IEEE International Conference on Control Applications, St. Petersburg, 2009, pp. 1368–1373. doi:10.1109/CCA.2009.5280933.

[8] I. Ulacia, J. Larrañaga, A. Arana, A. Iñurritegui, J. Elizegi, Fatigue life prediction of spherical gear couplings, in: American Gear Manufacturers Association Fall Technical Meeting 2018, Illinois, 2018, pp. 202–207.

[9] K. Mitome, T. Okuda, T. Ohmachi, T. Yamazaki, Development of a new hobbing of spherical gear, Transactions of the Japan society of mechanical engineers. Series C 66 (646) (2000) 1975–1980. doi:10.1299/kikaic.66.1975.

[10] L. Chao, C. Tsay, Contact characteristics of spherical gears, Mechanism and Machine Theory 43 (10) (2008) 1317–1331. doi:10.1016/j.mechmachtheory.2007.10.008.

[11] L. Kelemen, J. Szente, Two mathematical models for generation of crowned tooth surface, The Scientific World Journal 2014 (2014). doi:10.1155/2014/641091.

[12] A. Iñurritegui, I. Gonzalez-Perez, A. Arana, J. Larrañaga, I. Ulacia, Computerized generation and tooth contact analysis of spherical gear couplings for high misalignment applications, Mechanism and Machine Theory 164 (2021). doi:10.1016/j.mechmachtheory.2021.104408.

[13] J. Hong, D. Talbot, A. Kahraman, Effects of tooth indexing errors on load distribution and tooth load sharing of splines under combined loading conditions, Journal of Mechanical Design (2015). doi:10.1115/1.4029282.

[14] P. Renzo, S. Kaufman, D. de Rocker, Gear Couplings, Journal of Engineering for Industry (1968) 467–474.

[15] Y. Guan, X. Yang, Z. Fang, Computerized generation and simulation of meshing of a novel crown gear coupling avoiding edge contact, Journal of Advanced Mechanical Design, Systems, and Manufacturing 13 (3) (2019). doi:10.1299/jamdsm.2019jamdsm0055.

[16] American Gear Manufacturers Association, AGMA 945-1-B20: Splines – Design and Application (2020).

[17] International Organization for Standardization, ISO 4156: Straight cylindrical involute splines (2005).

[18] J. Hong, D. Talbot, A. Kahraman, Load distribution analysis of clearance-fit spline joints using finite elements, Mechanism and Machine Theory 74 (2014) 42–57. doi:10.1016/j.mechmachtheory.2013.11.007.

[19] W. Herbstritt, J. Paluh, Mill spindle advanced gear design, Iron and Steel Engineers 76 (7) (1999) 44–48.

[20] Deutsches Institut für Normung, DIN 5466: Splined joints, calculation of load capacity (2002).

[21] American Gear Manufacturers Association, AGMA 6123-B06: Design manual for enclosed epicyclic gear drives (2006).

[22] R. Beckmann, Beitrag zur Auslegung und Konstruktion von Balligzahn-Kupplungen, Ph.D. thesis, Chemmitz Technology University (2005).

[23] American Gear Manufacturers Association, AGMA 1102-A03: Tolerance Specification for Shaper Cutters (2010).

[24] F. Litvin, A. Fuentes, Gear geometry and applied theory, 2nd Edition, Cambridge University Press, 2004.

[25] G. Henriot, J. Boisset, Accouplements, Alignement des axes, in: Engrenages: conception, fabrication, mise en oeuvre, 5th Edition, Dunod, 1983, pp. 796–818.

[26] M. Octrue, F. Blanc, D. Ghribi, Guide de demensionnement des accouplements à dentures bombées, CETIM, 2014.

[27] D. Marano, M. Lorenzini, L. Mastrandrea, F. Pulvirenti, M. Turci, N. Fillault, Misalignment Compensation Spline Design, in: American Gear Manufacturers Association Fall Technical Meeting 2019, Dallas, 2019.

[28] V. Tran, R. Hsu, C. Tsay, Study on the anti-twist helical gear tooth flank with longitudinal tooth crowning, Journal of Mechanical Design 136 (6) (2014) 061007. doi:10.1115/1.4027166.

[29] L. Xiao, Y. Xu, X. Sun, H. Xu, L. Zhang, Experimental investigation on the effect of misalignment on the wear failure for spline couplings, Engineering Failure Analysis 131 (2022). doi:10.1016/j.engfailanal.2021.105755.

[30] J. Hong, A semi-analytical load distribution model of spline joints, Ph.D. thesis, The Ohio State University (2015).

[31] Y. Guan, J. Chen, H. Chen, S. Hu, X. Liu, An experimental investigation of contact characteristics of crown gear coupling with angular misalignment, Journal of Advanced Mechanical Design 5 (5) (2021). doi:10.1299/jamdsm.2021jamdsm0062.

[32] R. Cedoz, M. Chaplin, Design guide for involute splines, Society of Automotive Engineers, 1994.

[33] E. Neale, Introduction to gear couplings, Tech. rep., Neale consulting engineers (1980).

[34] S. Radzevich, Dudley's handbook of practical gear design and manufacture, 3rd Edition, CRC Press, Taylor & Francis group, 2016.

[35] R. Heinz, Untersuchung der Zahnkraft- und Reibungsverhältnisse in Zahnkupplungen, Konstruktion 12 (1978) 483–492.

[36] A. Andrew, Another efficient algorithm for convex hulls in two dimensions, Information Processing Letters 9 (5) (1979) 216–219. doi:10.1016/0020-0190(79)90072-3.
[37] International Organization for Standardization, ISO 21771: Gears-Cylindrical involute gears and gear pairs-Concepts and geometry (2007).
[38] B. De Caires, Variation analysis of involute spline tooth contact, Ph.D. thesis, Brigham Young University (2006).
[39] D. Dudley, How to design involute splines, Product Engineering (1957) 196–231.
[40] S. Medina, A. V. Olver, Regimes of contact in spline couplings, Journal of Tribology 124 (2) (2002) 351–357. doi:10.1115/1.1403456.
[41] N. Zafirah, A. Bakar, L. Ghee, H. Hussain, Reasarch on load distribution of different involute spline clearance, TEST engineering and mnagement 82 (2020) 3058–3068.